

Temperature biases in modeled polar climate and adoption of physical parameterization schemes

LIU Xiyong*, ZHAO Jiahua, XIA Huasheng, BAI Tonggui & ZHANG Tao

Institute of Meteorology, PLA University of Science and Technology, Nanjing 211101, China

Received 16 August 2011; accepted 11 January 2012

Abstract An annual cycle of atmospheric variations for 1989 in the Arctic has been simulated with the Weather Research and Forecasting (WRF) model. A severe cold bias was found around a cold center in surface air temperature over the Arctic Ocean, compared with results from ERA-Interim reanalysis. Four successive numerical experiments have been carried out to find out the reasons for this. The results show that the sea ice albedo scheme has the biggest influence in summer, and the effect of the cloud microphysics scheme is significant in both summer and winter. The effect of phase transition between ice and water has the biggest influence over the region near the sea ice edge in summer, and contributes little to improvement of the severe cold bias. The original crude albedo parameterization in the surface process scheme is the main reason for the large simulated cold bias of the cold center in summer. With a different land surface scheme than in the control run, cold biases of simulated surface air temperature over the Arctic Ocean are greatly reduced, by as much as 10 K, implying that the land surface scheme is critical for polar climate simulation.

Keywords polar climate, numerical simulation, WRF

Citation: Liu X Y, Zhao J H, Xia H S, et al. Temperature biases in modeled polar climate and adoption of physical parameterization schemes. *Adv Polar Sci*, 2012, 23:30-40, doi:10.3724/SP.J.1085.2012.00030

0 Introduction

The climate is changing in the Arctic and is predicted to change at a rate significantly faster than the planet as a whole in the near future, because of the influence of feedbacks related to human greenhouse gas emission and the changing Arctic Ocean surface^[1-2]. As discussed in several recent publications, both sea ice areal extent and thickness are decreasing at an alarming rate^[3-5]. Sound quantitative understanding of these interactions is essential to the development of predictive capability for the future atmospheric state in the Arctic, and how this relates to global climate change^[6]. However, understanding the fundamentals of associated surface chemical, physical and biological exchange processes occurring at relevant interfaces in the Arctic is weak^[7]. Thus, climate mechanisms in the Arctic

are active research topics, and our understanding of their causes and effects is far from complete.

One of the most complicated but fascinating problems in polar climate change is whether atmosphere or sea ice is dominant within the warming process. Some studies support the idea that, for variations on interannual or decadal scales, atmospheric changes drive variations in sea ice^[8-9]. By analyzing the ERA-Interim reanalysis dataset, it was recently asserted that diminishing sea ice had a leading role in recent Arctic temperature amplification^[10].

Since numerical models provide an ideal environment for testing the importance of critical processes in a controlled manner, the Arctic research community benefited from an explosive growth in numerical modeling at the close of the twentieth century. With numerical models, scientists can test their ideas and explore new theories on Arctic research. To understand the “atmosphere vs. sea ice problem” mentioned above, scientists have designed different numerical experiments. These are either sea ice and ocean forcing the atmospheric model, or the atmosphere forcing the ocean-sea ice coupled model. A precondition is

*Corresponding author (born in 1970, male, Ph.D., Associate Professor, majored in climate simulation of high latitudes, email: liuxy@ome.ac.cn)

to have a reliable numerical model. Since mesoscale regional climate models provide finer resolution and perform numerical experiments more efficiently, they have been recognized as an increasingly important tool to address scientific issues associated with climate variability and impacts at local and regional scales^[11-12]. Many regional climate models have been developed, applied, and compared, demonstrating the achievement of important downscaling skills and model deficiencies yet unresolved^[13-15].

The Weather Research and Forecasting (WRF) model^[16] can be downloaded from www.mmm.ucar.edu/wrf/users/download/get_source.html. It is a numerical weather prediction and atmospheric simulation system designed for both research and operational applications. It is suitable for a broad span of applications across scales from large-eddy to global simulation, although it was initially developed for regional applications^[17]. Since the model has much merit for numerical simulation, it seems fitting to extend it to polar climate research. Although there are studies using a prior version of WRF in regional climate simulation outside polar regions^[15,17], there is no formal publication on the application of the WRF (version 3.2.1) extension to polar climate research. Based on WRF version 2.2, a Polar WRF (PWRf) has been developed and used in research on Arctic weather^[18]. A PWRf based on WRF version 3.3.1 is now available.

Using the WRF model with extension for polar climate, we perform numerical experiments with different configurations of physical parameterization schemes to explore improvements to polar climate simulation. In section 1, we introduce the polar climate extension for WRF and the numerical experiment design. In section 2, we do an analysis to understand the cold bias of surface air temperature near the Arctic Ocean cold center in the simulation results. The last section is a summary and discussion.

1 Model and design of numerical experiments

1.1 Model

The WRF 3.2.1 with polar climate extension (WRF/PCE)^[19-20] is used for the numerical experiments. Compared to WRF, the WRF/PCE includes some modifications suitable for polar climate applications. These modifications are:

(a) Improvement in physical parameterization schemes associated with sea ice

Since sea ice partially covers the Arctic ocean, proper depiction of sea ice effects is very important in polar climate simulation. The sea ice albedo parameterization scheme in WRF/PCE is improved to characterize the melt effect of sea ice on albedo; the sea ice albedo is reduced from 0.7 in the Arctic spring/fall to 0.55 in melt season. To depict the effect of sea ice nonhomogeneity, a flux aggregation scheme is used to calculate surface heat and radiation fluxes for grids with sea ice (surface fluxes are calculated for water and sea ice separately, then average values with

areal weighting are used).

(b) Addition of interface for ERA-Interim dataset in WRF Pre-Processing System (WPS) and update of bottom boundary condition during integration

Fields from the ERA-Interim dataset^[21] are used as model initial values and boundary conditions. Since data downloaded from the ERA-Interim dataset are saved in netCDF format, they must be transformed into binary format for ingestion by the WPS metgrid program. Thus, an interface program for the ERA-Interim dataset in the WPS is introduced, to execute this transformation. A bottom-boundary update function is introduced to mimic the mechanism of lateral boundary update. Sea ice concentration, vegetation fraction, sea surface temperature, leaf area index and background albedo can be changed at given intervals.

(c) Other technical arrangements

To save disk space and facilitate data analysis, a monthly mean calculation and monthly data output function were added. To simplify calculation and output of monthly mean data, date calculation code was modified so each month is 30 d in the model.

WRF/PCE inherits all WRF numerical weather prediction functionalities as developed at NCAR (National Center for Atmospheric Research), with additions and modifications ((a) through (c) above) for polar climate simulation. The dynamics and physics of WRF/PCE are identical to WRF, except for one land surface model modified for polar climate application, as mentioned in (a). The WRF solves fully-compressible Euler nonhydrostatic equations. We adopted a time-split integration using a 2nd- or 3rd-order Runge-Kutta scheme with smaller time step for acoustic and gravity-wave modes. Model physics include microphysics, cumulus parameterization, surface physics, planetary boundary layer physics and atmospheric radiation physics, each with a choice of multiple schemes. For details of WRF dynamics and physics, refer to the WRF technical note for version 3^[16].

1.2 Model grid

WRF/PCE uses a staggered horizontal grid (Arakawa C-grid) with a vertical terrain-following η coordinate defined by dry hydrostatic pressure and with vertical grid stretching permitted. The model domain consists of 160 grid points in the east-west direction and 100 grid points in the south-north direction, for variables other than wind components. The domain is centered at 90°N and 0°E, with horizontal grid spacing 50 km on the polar stereographic mapping plane. Twenty-seven η levels are used, of which close to eight are within the planetary boundary layer. The pressure at model top is about 50 hPa.

1.3 Initial and boundary condition

Initial and boundary condition data, sea surface temperature and sea ice concentration are all from the 3-hourly, 1.5° ERA-Interim reanalysis dataset, which is the next genera-

tion of the ERA-40 dataset^[21]. The key improvements of ERA-Interim over ERA-40 include higher resolution, improved model physics, better hydrologic cycle, four-dimensional variational data assimilation, and variational bias correction of satellite radiance data. ERA-Interim provides more accurate Arctic tropospheric temperatures, and probably has fewer spurious trends than previous reanalysis datasets^[22].

The lateral boundary conditions of wind in two directions, geopotential height, temperature and water vapor mixing ratio are interpolated directly from ERA-Interim. Lateral boundary values of vertical velocity, cloud water, ice and snow mixing ratios are set to zero. The width of the lateral boundary is five grids. Fields for the lower boundary condition of sea ice concentration, sea surface temperature and vegetation fraction are also interpolated directly from ERA-Interim. The lateral and lower boundary conditions can all be updated at given intervals (e.g., 6 h).

We used the 10-minute-resolution dataset for topography, land use and soil type.

1.4 Design of numerical experiments

We designed five numerical experiments (Table 1). EXP1 was a control run for comparison. In EXP2, EXP3, EXP4 and EXP5, each configuration was varied slightly over EXP1 for a special purpose. In EXP1, the model used the WRF Single-Moment 3-class (WSM3) microphysics scheme, in which mixed-phase processes are not considered. Transformation processes between sea ice points and water points are also not considered. EXP1 used the Noah Land Surface Model (LSM), in which sea ice albedo is made constant. Other major configurations in EXP1 included the Rapid Radiation Transfer Model (RRTM) scheme for long wave radiation, the Dudhia scheme for solar radiation, the Monin-Obukhov scheme for near-surface processes, and the Yonsei University (YSU) scheme for the boundary layer.

Modulation of Arctic sea ice conditions has been recognized as a potentially significant climate feedback mechanism for two primary reasons, namely, albedo modification and impact on energy transfer across the air-sea interface^[23]. The phase transformation process between water and sea ice occurs mostly near the sea ice edge. In EXP2, transformation processes between sea ice points and water points are considered. If updated sea ice concentration is greater than a critical value (set to 0.02 in the model), the underlying surface type changes to ice with partial water. If this updated concentration is smaller than the critical value, the underlying surface type changes to water. If the underlying surface type is ice with partial water, values of surface albedo and emissivity are averages of ice and water. Clouds have a significant effect on global albedo and are important in the hydrologic cycle. Though mixed phase clouds are less understood, they are important since they are the main precipitating clouds and cover a substantial portion of the earth surface. Further, mixed-phase cloud processes are critical to precipitation development. To study

the influence of mixed-phase clouds on Arctic climate, an Eta grid-scale cloud and precipitation scheme for microphysics, in which mixed-phase processes are considered, is used in EXP3. In addition to the inclusion of transformation processes between sea ice points and water points in EXP4, sea ice albedo parameterization within the Noah LSM^[24] is improved. In the original code, the albedo of sea ice remains a constant value that is suitable for winter. In the improved sea ice albedo parameterization scheme, sea ice albedo is reduced from 0.7 in Arctic spring/fall to 0.55 in melt season, for characterizing the melt effect of sea ice on albedo. Since sea ice cover is usually treated as a land surface type in atmospheric models, the LSM is a great contribution to climate model results, especially in the lower atmosphere. To study the effects of land surface processes in EXP5, the Pleim-Xiu LSM^[25] with greater consideration of sea ice nonhomogeneity is used, instead of the Noah LSM.

Table 1 List of numerical experiments

Name	Description
EXP1	WSM3 microphysics, transformation processes between sea ice points and water points are not considered, Noah land surface model, RRTM scheme for long wave radiation, DUDHIA scheme for solar radiation, Monin-Obukhov scheme for near surface processes and YSU scheme for boundary layer, Kain-Fritsch cumulus scheme are considered.
EXP2	Same as EXP1, except that transformation processes between sea ice points and water points are considered.
EXP3	Same as EXP1, except that an Eta grid-scale cloud and precipitation scheme for microphysics is used.
EXP4	Same as EXP2, except that sea ice albedo parameterization in Noah land surface model is improved.
EXP5	Same as EXP1, except that Pleim-Xiu land surface model with improved consideration of sea ice nonhomogeneity is used.

A time step of 180 s is used, and width of the relaxation zone is set to 4 grids for sponge lateral boundary treatment in all experiments. All configured experiments had an initiation time of 0000 UTC on 1 January 1989, and were integrated over a year. During integration, both lateral and bottom boundaries were updated every 6 h. Except for explicit indications, default values in the namelist file were used.

2 Analysis of simulation results

2.1 Results from control run (EXP1)

2.1.1 Sea level pressure and geopotential height

The main features of annual mean sea-level pressure are a low-pressure trough extending northward along the Norway and Barents Seas, and a high-pressure zone near the Beau-

fort and Eastern Siberia Seas (Figure 1a). Compared with ERA-Interim results, the simulated low-pressure trough is weaker, with a maximum difference of nearly 3.5 hPa. The

feature of a stronger high-pressure zone with biases 1–4 hPa (Figure 1b).

As shown in Figure 2a, the main feature of annual mean

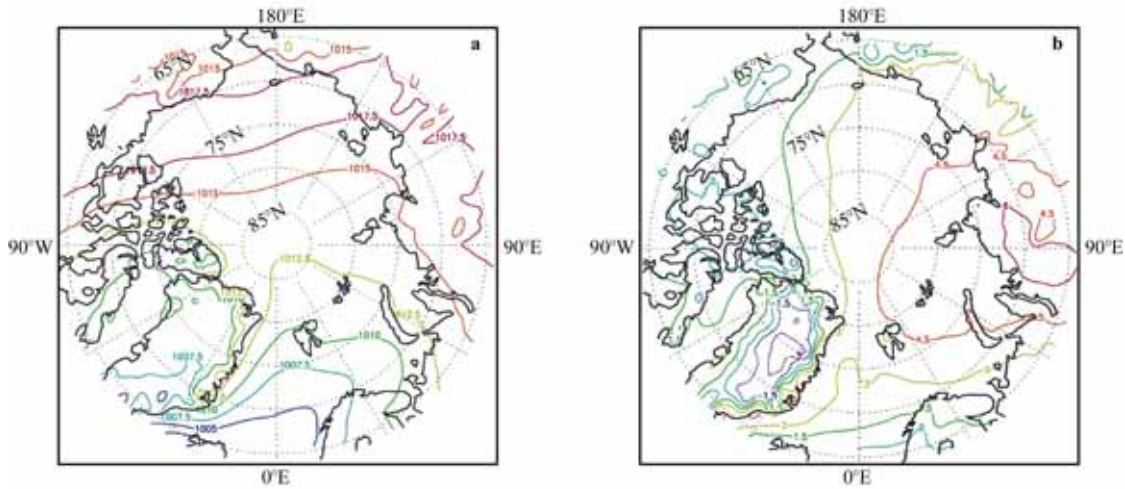


Figure 1 Annual mean sea-level pressure over ocean. **a**, Result of EXP1, contour interval 2.5 hPa. **b**, Result of EXP1 minus ERA-Interim, contour interval 1.5 hPa.

geopotential height at 500 hPa is the polar vortex. In ERA-Interim, the vortex center is near the North Pole, whereas in EXP1 there is an extra vortex center near Baffin Bay. Compared with ERA-Interim results (Figure 2b), simulated geopotential height at 500 hPa is low, and the big

difference near Baffin Bay results in the false center of closed circulation in Figure 2a (wind vectors not shown). The distribution of geopotential height and wind obey the wind-pressure law.

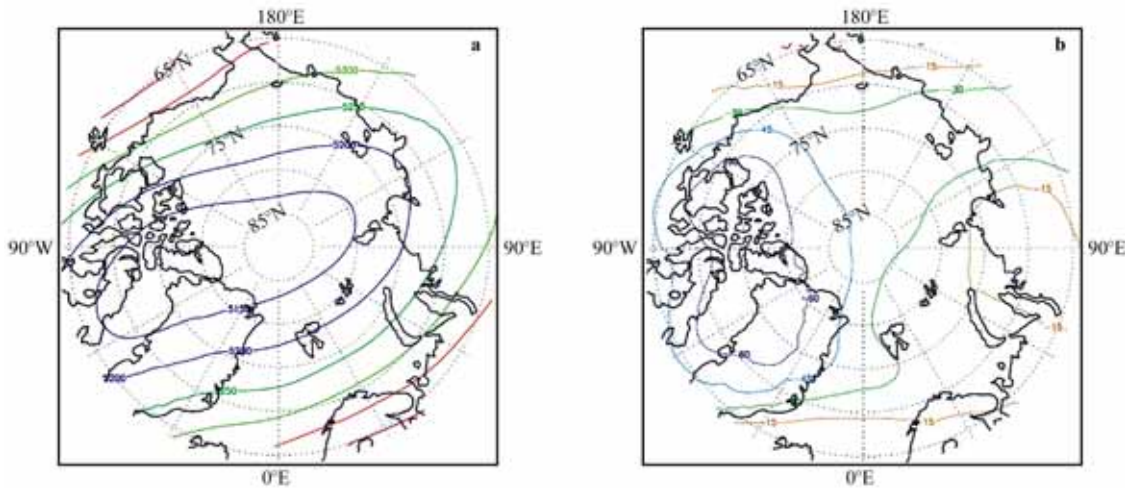


Figure 2 Annual mean geopotential height at 500 hPa. **a**, Result of EXP1, contour interval 50 gpm. **b**, Result of EXP1 minus ERA-Interim, contour interval 15 gpm.

2.1.2 Temperature

In January, there are two main cold centers of surface air temperature (SAT, represented by air temperature at 2 m): one over the Arctic Ocean and another over Greenland. The model reproduced the two cold centers well, but produced another false cold center over the ice-covered region of Baffin Bay (Figure 3a). In fact, there are two more false cold centers, one over Hudson Bay and another over Foxe

Basin, shown in Figure 3a. The model reproduced warm ridges over the Labrador and the Norwegian Seas (also in Figure 3a). Compared with ERA-Interim results, most areas have a cold bias, including all ice-covered areas (Figure 3b). The two main cold centers of simulated surface air temperature are colder than ERA-Interim by more than 20 K and 10 K (Figure 3b). In July, the two main cold centers over the Arctic Ocean and Greenland still exist (Figure 3c). Except for the North Siberian lowland, compared with

ERA-Interim results, most areas have a cold bias, the larg-

est of which is over 10 K (Figure 3d).

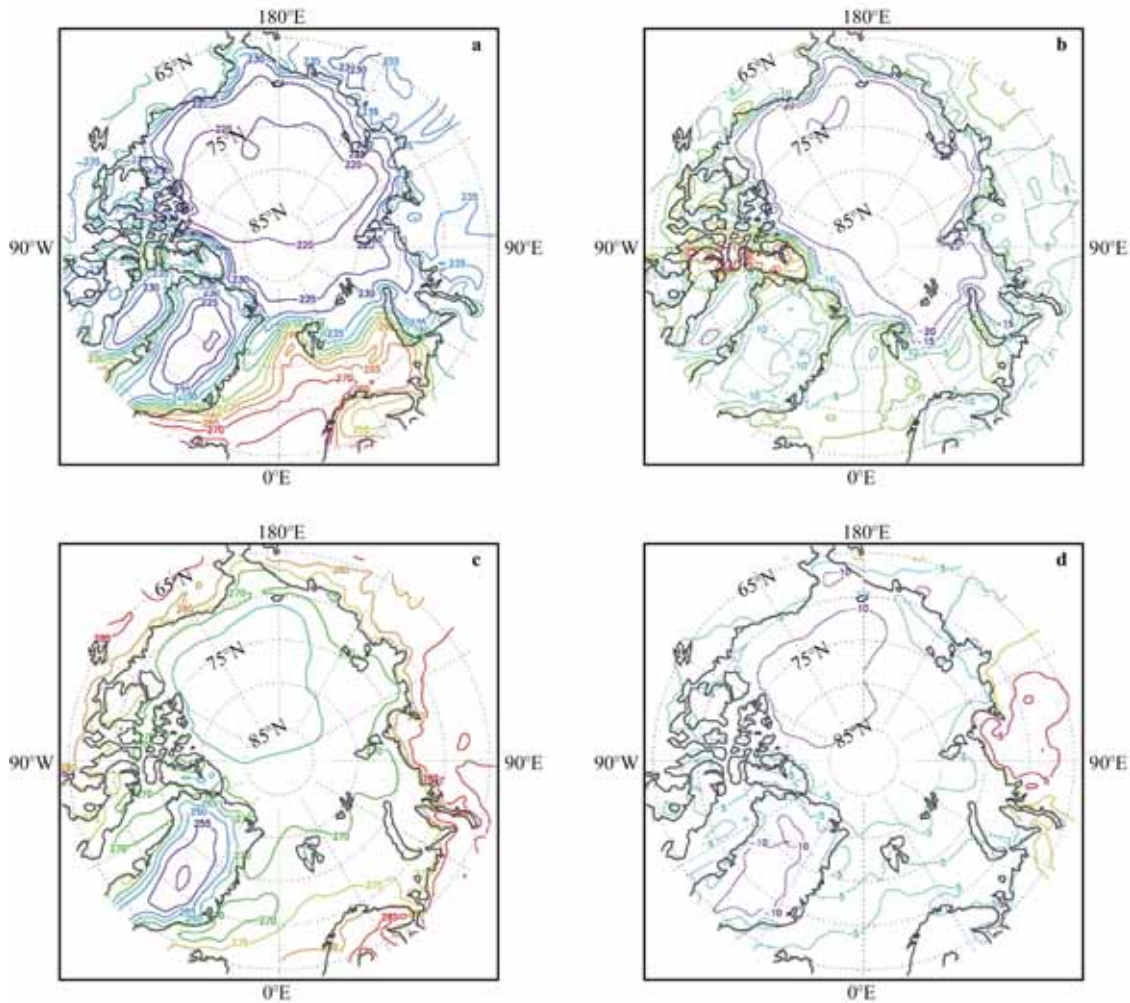


Figure 3 Simulated SAT of EXP1, and SAT difference between EXP1 and ERA-Interim (EXP1 minus ERA-Interim). **a**, EXP1 result for January. **b**, Difference for January. **c**, EXP1 result for July. **d**, Difference for July. Contour intervals are 5 K.

In January, the major cold center is over Greenland, with a cold belt extending to Eastern Siberia at 700 hPa, as shown in Figure 4a. Compared with ERA-Interim results, there is a large cold bias over Greenland, which is mainly because of displacement of the simulated cold center (Figure 4b). In July, there is a cold belt stretching from Greenland to Eastern Siberia, with the cold center over the Arctic Ocean (figure not shown). However, the simulated cold center at 700 hPa is over Greenland (Figure 4c). From the temperature difference figure (Figure 4d), cold biases are evident over nearly the entire domain. The biggest bias is over Greenland because of the false cold center there (Figure 4c). Since the 700 hPa level is below the surface in parts of Greenland, the temperature values there are extrapolated, with a dependence on the extrapolation method.

2.2 Effect of phase transition between ice and water

In EXP1, the effect of phase transition between ice and water is not considered. When this effect is added in EXP2,

two patches of SAT warm bias appeared in January. One was over the sea south of the Svalbard Islands, and another over the Barents Sea (Figure 5a). With reduced sea ice extent in the sea-ice border area because of the phase transition introduction, there is more upward sensible heat flux and vapor flux toward the atmosphere. The increased atmospheric water vapor contributes to greater stratus formation and long wave radiation trapping. These warm biases originate from increased downward long wave radiation in EXP2 (figure not shown). Comparing Figure 3b, it is evident that the warm biases contribute to simulation improvement. In July, by adding the effect of phase transition between ice and water, SAT in the Greenland, Barents and Chukchi Seas increases significantly (Figure 5b). Comparing Figure 3d, an improved simulation was also evidenced by increased temperature over those areas. There is an obvious temperature decrease over the North Siberian lowland, which improves model results (comparing Figure 5b with Figure 3d). This temperature decrease is connected with

decrease of downward long wave radiation in EXP2 (figure not shown). It is clear that the effect of phase transition

between ice and water contributes little improvement to the severe cold bias of the control run.

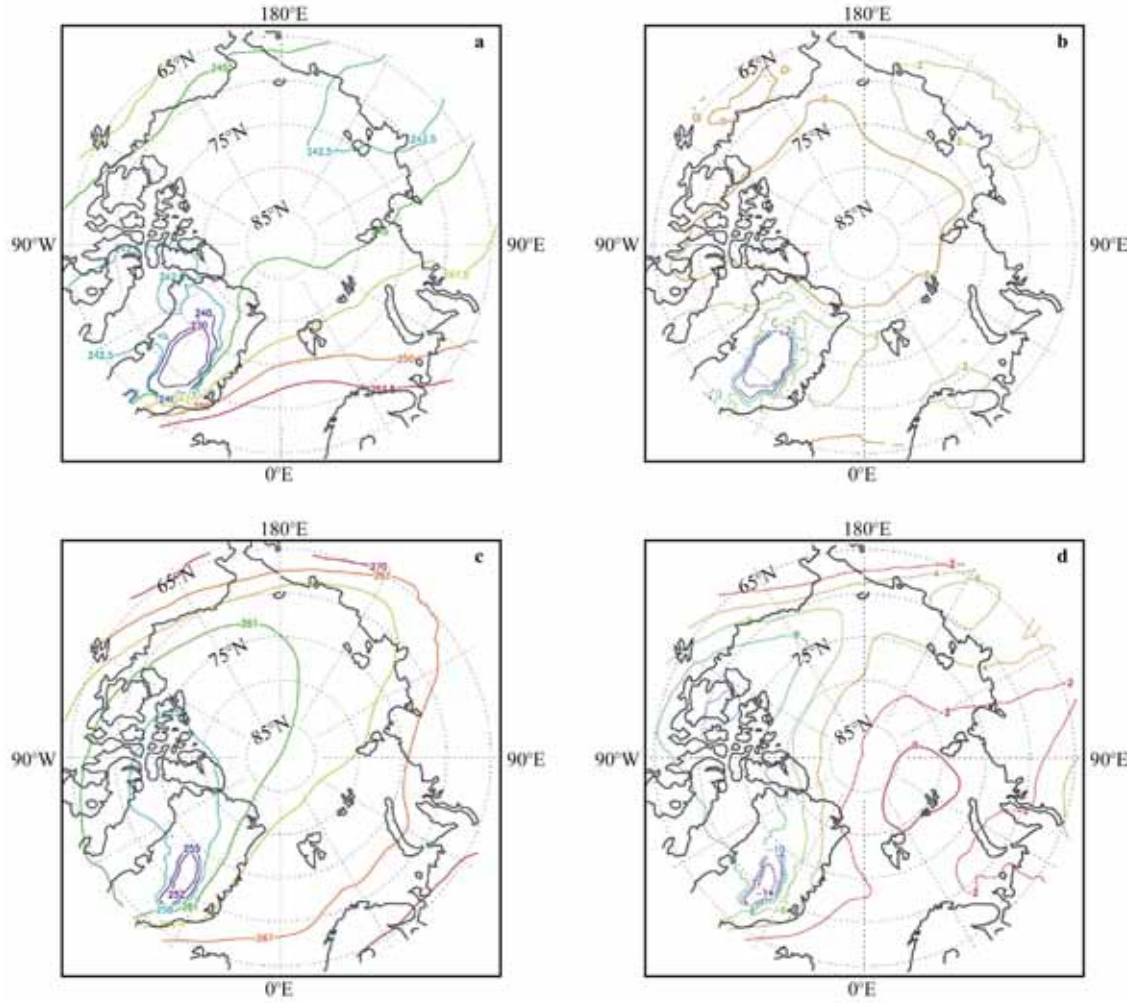


Figure 4 Same as Figure 3, except for temperature at 700 hPa. Contour levels for **a** are 230 K, 240 K, 242.5 K, 245 K, 247.5 K, 250 K and 252.5 K; contour interval for **b** is 2 K and lines for colder than -10 K are not drawn; contour interval for **c** is 3 K; and contour interval for **d** is 2 K.

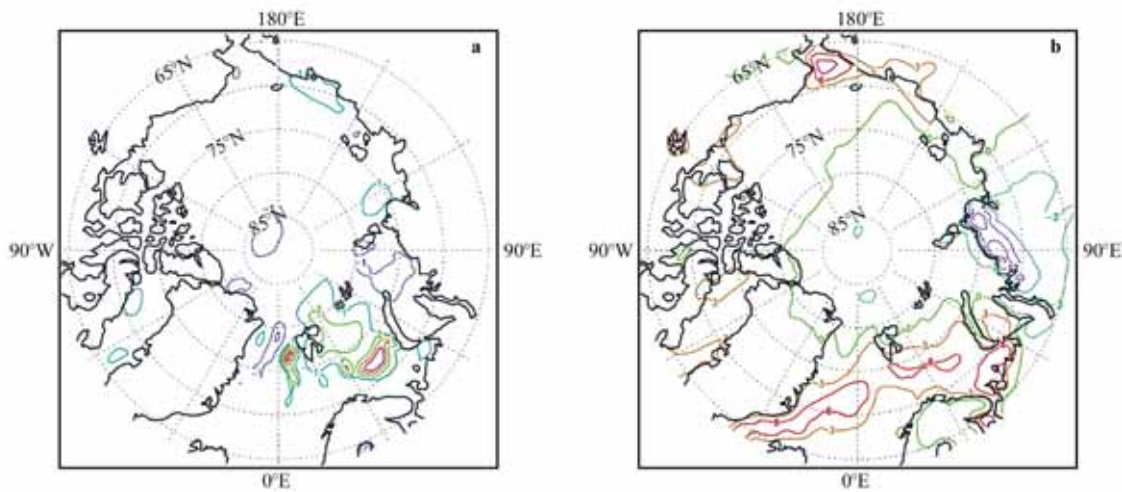


Figure 5 Simulated SAT difference (EXP2 minus EXP1). **a**, Result for January, contour interval 1 K. **b**, Result for July, contour interval 3 K.

In January, the simulated temperature difference at 700 hPa between EXP2 and EXP1 is small, with a maximum difference roughly 1 K (Figure 6a). In July, the greatest simulated cold bias between EXP2 and EXP1 is over 4 K, and greatest warm bias over 2 K (Figure 6b). The fact

that temperature difference range at 700 hPa is smaller than that at the surface is rational, since the source of the temperature difference is the surface (compare Figure 6 to Figure 5). A comparison of Figure 6b to Figure 4d shows that the cold bias worsens model results in EXP2.

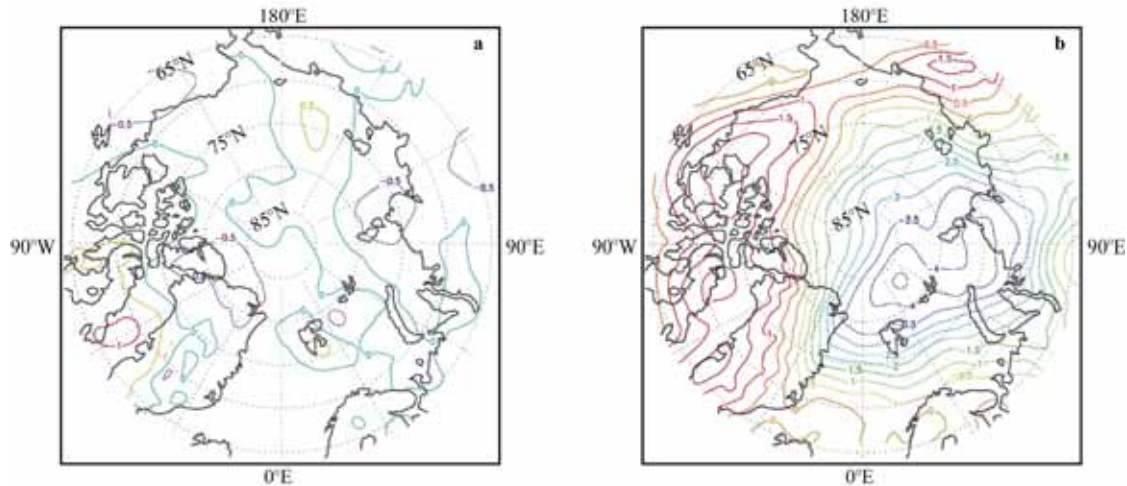


Figure 6 Simulated temperature difference at 700 hPa (EXP2 minus EXP1). **a**, Result for January. **b**, Result for July. Contour intervals are 0.5 K.

2.3 Effect of cloud microphysics scheme

The simulated cloud has a close connection with the cloud microphysics scheme used. Since the type and amount of cloud can influence model radiation calculation, this scheme will affect the simulation result. The WSM3 microphysics scheme includes ice sedimentation and other new ice-phase parameterizations. It predicts three categories of hydrometers: vapor, cloud water/ice, and rain/snow. This is a so-called simple-ice scheme. The Eta grid-scale cloud and precipitation scheme predicts changes in water vapor and condensate in the forms of cloud water, rain, cloud ice and precipitation ice (snow/graupel/sleet). The individual hydrometeor fields are combined into total condensate, and water vapor and total condensate are advected in the model. In January, major differences of SAT from the two different cloud microphysics schemes are shown in Figure 7a. Except for the warm bias over the southern Barents Sea, almost all significant biases can be attributed to differences in downward long wave radiation (Figure 8a). The warm bias over the southern Barents Sea, where downward long wave radiation flux bias is negative, is caused by reduced loss of sensible heat flux from the ocean surface (Figure 9a). In July, surface downward longwave radiation is still important in temperature variation, through modulating the heat balance controlling SAT variation. Except for cold biases in the Arctic Ocean near 85°N, almost all SAT biases are closely tied to differences of downward long wave radiation flux (Figures 7b and 8b). These cold biases are mainly generated by the decrease of downward shortwave radiation flux, with values in excess of $20 \text{ W}\cdot\text{m}^{-2}$ (Figures 7b and 9b).

Simulated temperature differences between EXP3 and EXP1 at 700 hPa show larger biases in summer (figures not shown).

2.4 Effect of sea ice albedo parameterization

Albedo is a non-dimensional, unitless quantity that indicates how effectively a surface reflects solar energy. Sea ice has a much higher albedo than other earth surfaces, such as the surrounding ocean. A typical ocean albedo is approximately 0.06, whereas bare sea ice varies from approximately 0.5 to 0.7. When sea ice albedo parameterization is improved (sea ice albedo variation with season, and albedo reduction effect considered during melt season), there is little influence on SAT distribution in January (Figures 5a and 10a). This is because downward shortwave radiation flux is small at high northern latitudes in winter. The situation is different in summer. Because of the introduction of decreased sea ice albedo within the scheme, the earth surface absorbs more shortwave radiation and this increased downward shortwave radiation warms the sea ice surface, so this ice begins to melt. During the melt process, the ice surface temperature remains freezing point and the near-surface air temperature does not change much. Before the onset of ice melt, albedo strongly affects the surface heat balance and consequent feedback to the near-surface air temperature. If the sea ice has melted, the open ocean receives more downward radiation and its water is warmed. The warmed ocean surface then increases SAT (compare Figure 10b with Figure 5b).

In addition, simulated temperature differences between EXP4 and EXP1 at 700 hPa in summer are greater than in

winter (figures not shown).

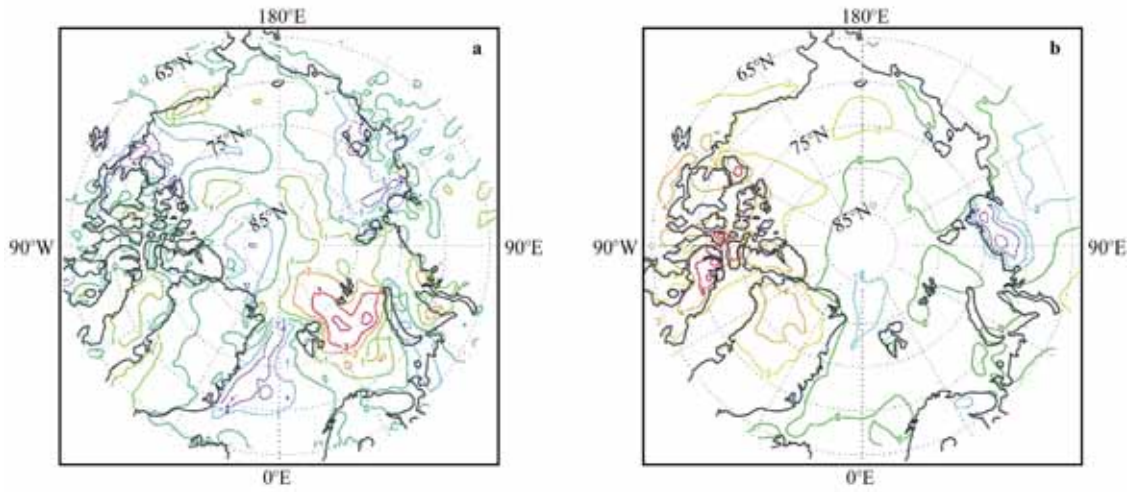


Figure 7 Simulated SAT difference (EXP3 minus EXP1). **a**, Result for January, contour interval 1 K. **b**, Result for July, contour interval 2 K.

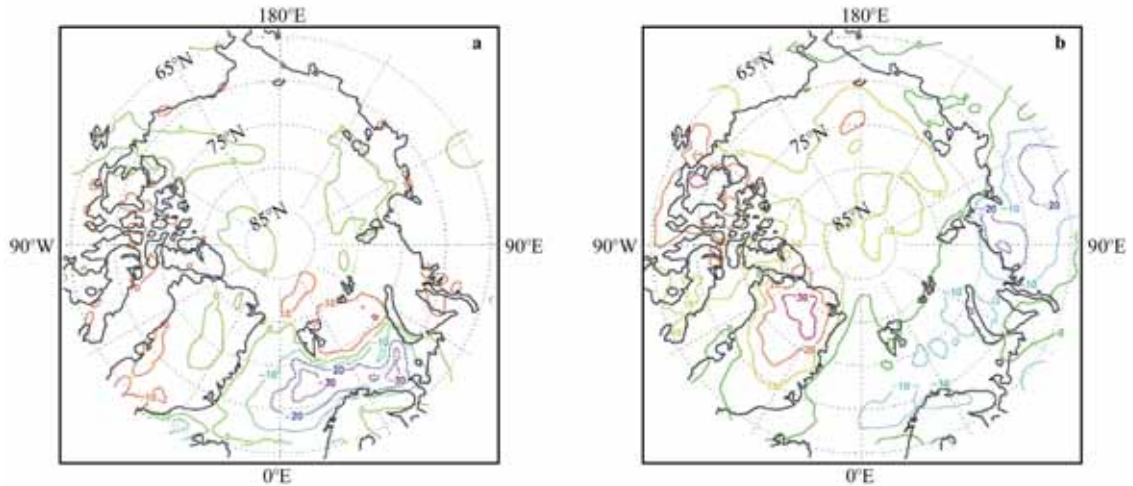


Figure 8 Simulated downward long wave radiation flux difference (EXP3 minus EXP1). **a**, Result for January. **b**, Result for July. Contour intervals are $10 \text{ W}\cdot\text{m}^{-2}$.

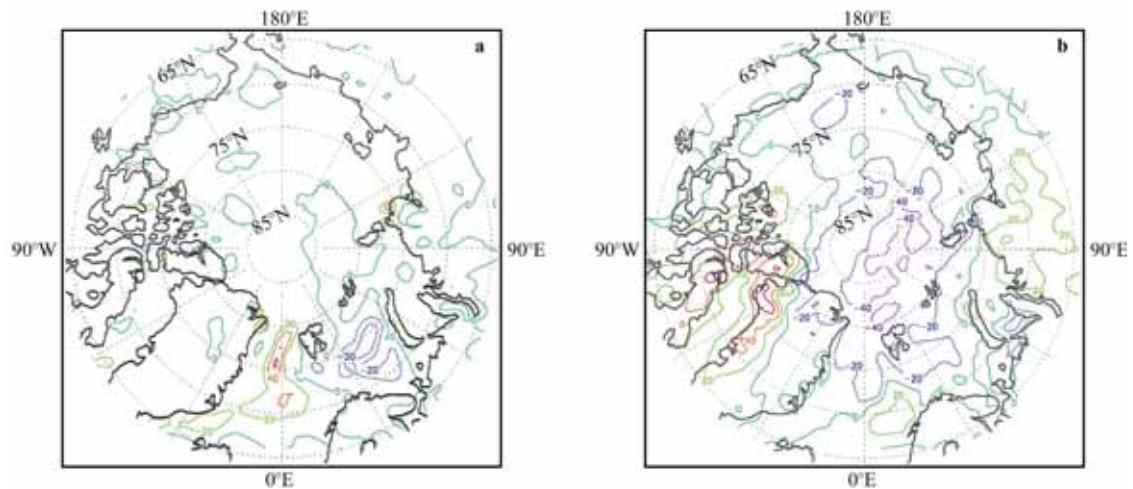


Figure 9 Simulated differences of upward sensible heat flux and downward shortwave radiation flux (EXP3 minus EXP1). **a**, Upward sensible heat flux in January. **b**, Downward shortwave radiation in July. Contour intervals are $20 \text{ W}\cdot\text{m}^{-2}$.

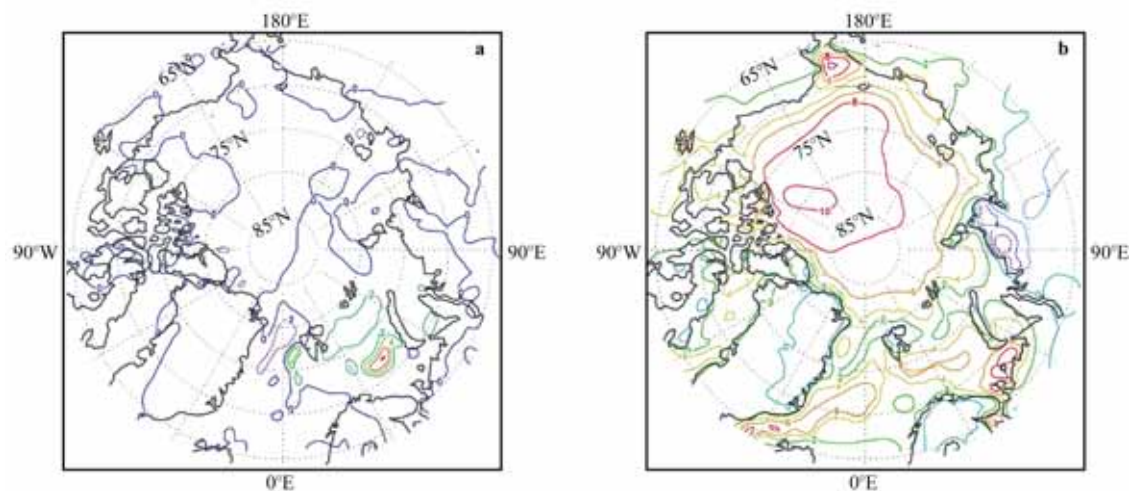


Figure 10 Simulated SAT difference with different sea ice albedo parameterization scheme (EXP4 minus EXP1). **a**, Result for January. **b**, Result for July. Contour intervals are 2 K.

2.5 Effect of land surface processes

Studies show that modeled results are sensitive to the choice of LSM^[26–27]. To improve polar climate simulation, it is helpful to explore this sensitivity.

The Pleim-Xiu LSM greatly improves SAT simulation, compared with Noah LSM use (Figures 11 and 4). In January, the SAT difference between model results of EXP5 and ERA-Interim is no more than 10°C in most areas (Figure 11c). In summer, the biggest SAT difference between model results and ERA-Interim is no more than 6°C over the ocean (Figure 11d). Biases over the ocean are all negative (Figures 11b and 11d). Nevertheless, there is a larger warm bias over the North Siberian lowland in July (Figures 11d and 3d). The results of EXP1 and EXP5 show that the proper LSM or LSM improvement is critical for polar climate simulation.

At 700 hPa, temperature differences between EXP5 and EXP1 are smaller than for the SAT over the Arctic Ocean (figures not shown). There are more surface downward longwave radiation fluxes over the ocean in EXP5, compared to EXP1 (figures not shown).

3 Summary and conclusions

Using WRF 3.2.1 with extension for polar climate, an annual cycle of atmospheric variations for 1989 in the Arctic was simulated with different configurations of physical parameterization schemes. We analyzed the influences of land surface schemes, sea ice albedo, transformation processes between sea ice points and water points, and cloud microphysics on polar climate simulation. The model reproduced two cold centers over the Arctic Ocean and Greenland, with decreased SAT. It also faithfully reproduced warm ridges over the Labrador and Norwegian Seas in January. In July, simulated SAT over most areas shows a cold bias. This bias may be severe for certain configurations of physical parameterization schemes. In summer, the sea

ice albedo scheme has the biggest influence on SAT simulation over inner parts of the Arctic Ocean. The effect of phase transition between ice and water has the biggest effect on SAT simulation near the sea ice edge, and contributes little to improvement of the severe cold bias over the Arctic Ocean. The effect of the cloud microphysics scheme is significant in both winter and summer. Through land surface model substitution, the previous large cold bias over Greenland in both summer and winter, and those over the Arctic Ocean in winter, can be greatly reduced, by as much as 10 K. Since sea ice cover is usually treated as a land surface type in atmospheric models and the effect of sea ice is important at high latitudes, a LSM strongly contributes to climate model results. A suitable LSM or LSM improvement is critical for polar climate simulation.

The Arctic is a major region in the global climate. Thorough understanding of its role requires that we account for the intimate coupling between Arctic atmosphere, land, ocean and sea ice^[1]. Prior to this, we must clarify atmospheric behavior given varying sea ice distribution, the physical parameterization scheme in numerical models, and other factors. The subject of temperature biases was addressed here through numerical experiment, revealing that there are still many uncertainties. These must be determined and reduced in the simulation of polar climate. The PWRP has been validated for synoptic cases in Greenland and the Arctic Ocean, giving promising results^[18]. Thus, it would be valuable to tune model parameters in the Noah land surface scheme using methods within the PWRP model, or to develop a PWRP climate extension version and do further study.

Acknowledgments The work is cosponsored by the Natural Science Foundation of China (Grant no. 40876101) and the National High Technology Research and Development Program of China (863 Program) (Grant no. 2010AA012304). The ERA-Interim reanalysis dataset was downloaded from the ECMWF data server website. Comments from two anonymous reviewers helped to improve the manuscript.

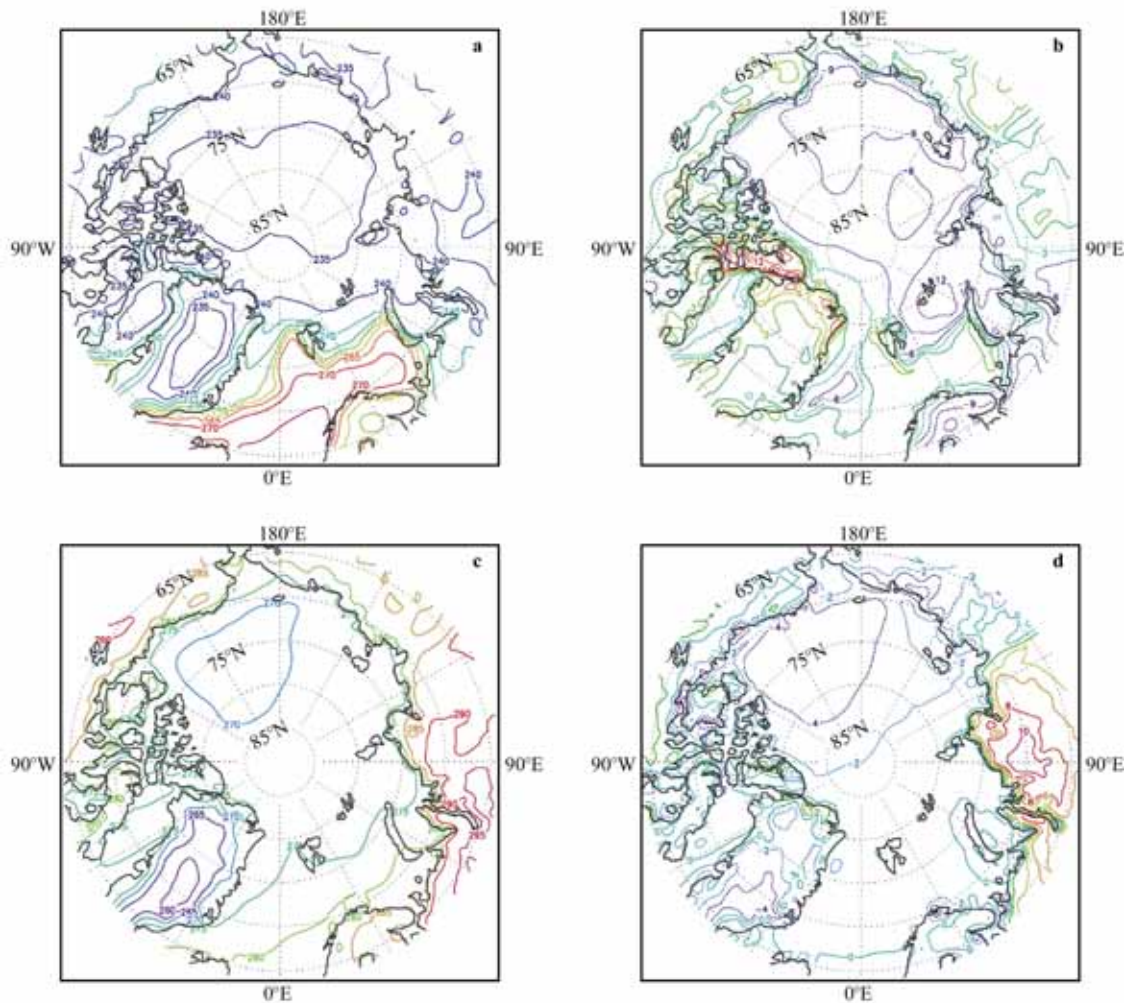


Figure 11 Simulated SAT in EXP5, and SAT difference between EXP5 and ERA-Interim (EXP5 minus ERA-Interim). **a**, EXP5 result for January. **b**, Difference for January. **c**, EXP5 result for July. **d**, Difference for July. Contour intervals are 5 K for **a** and **c**, 3 K for **b**, and 2 K for **d**.

References

- 1 Serreze M C, Francis J A. The Arctic amplification debate. *Climate Change*, 2006, 76: 241-264.
- 2 Thorne P W. Arctic tropospheric warming amplification. *Nature*, 2008, 455: E1-E2.
- 3 Stroeve J, Holland M M, Meir W, et al. Arctic sea ice decline: faster than forecast. *Geophysical Research Letters*, 2007, 34 (L09501), doi:10.1029/2007GL029703.
- 4 Lindsay R W, Zhang J, Schweiger A, et al. Arctic sea ice retreat in 2007 follows thinning trend. *Journal of Climate*, 2009, 22: 165-176.
- 5 Kwok R, Rothrock D A. Decline in Arctic sea ice thickness from submarine and ICESat records: 1958–2008. *Geophysical Research Letters*, 2009, 36 (L15501), doi:10.1029/2009GL039035.
- 6 Higgins M E, Cassano J J. Impacts of reduced sea ice on winter Arctic atmospheric circulation, precipitation and temperature. *Journal of Geophysical Research*, 2009, 114 (D16107), doi:10.1029/2009JD011884.
- 7 Winton M. Amplified climate change: what does surface albedo feedback have to do with it. *Geophysical Research Letters*, 2006, 33 (L03701), doi:10.1029/2005GL025244.
- 8 Deser C, Walsh J E, Timlin M S. Arctic sea ice variability in the context of recent atmospheric circulation trends. *Journal of Climate*, 2000, 13: 617-633.
- 9 Liu X Y, Liu H L, Li W, et al. Numerical simulation of atmosphere-ocean-sea ice interaction during interannual cycle in high northern latitudes. *Acta Meteorologica Sinica*, 2008, 22: 119-128.
- 10 Screen J A, Simmonds I. The central role of diminishing sea ice in recent Arctic temperature amplification. *Nature*, 2010, 464: 1334-1337.
- 11 Leung L R, Mearns L O, Giorgi F, et al. Regional climate research. *Bulletin of American Meteorology Society*, 2003, 84: 89-95.
- 12 Liang X Z, Choi H, Kunkel K E, et al. Surface boundary conditions for mesoscale regional climate models. *Earth Interactions*, 2005, 9: 1-28.
- 13 Takle E S, Gutowski W J, Arritt R W, et al. Project to intercompare regional climate simulations (PIRCS): Description and initial results. *Journal of Geophysical Research*, 1999, 104: 19443-19461.
- 14 Roads J, Chen S, Cocke S, et al. International Research Institute/Applied Research Centers (IRI/ARCs) regional model intercomparison over South America. *Journal of Geophysical Research*, 2003, 108: 4425, doi:10.1029/2002JD003201.
- 15 Zhang Y X, Duliere V, Mote P, et al. Evaluation of WRF and HadRM Mesoscale Climate Simulations over the United States Pacific Northwest. *Journal of Climate*, 2009, 22: 5511-5526.
- 16 Skamarock W, Dudhia J, Gill D O, et al. A Description of the Advanced

- Research WRF version 3. NCAR Technical Note, NCAR/TN-475+STR, 2008.
- 17 Melissa S B, Karoly D J. Precipitation simulations using WRF as a nested regional climate model. *Journal of Applied Meteorology and Climatology*, 2009, 48: 2152-2159.
- 18 Bromwich D H, Hines K M, Bai L S. Development and testing of Polar Weather Research and Forecasting model: 2. Arctic Ocean. *Journal of Geophysical Research*, 2009, 114 (D08122), doi:10.1029/2008JD010300.
- 19 Xia H S, Liu X Y. Numerical simulation of Arctic climate with the improved WRF model. *Proceedings of 2010 International Conference on Remote Sensing*, IEEE Inc, 2010, 3: 577-582 (in Chinese with English abstract).
- 20 Xia H S. Numerical simulations of the impact of sea ice and external atmospheric changes on the Arctic climate. Nanjing: PLA University of Science and Technology, 2011 (in Chinese with English abstract).
- 21 Simmons A, Uppala S, Dee D, et al. ERA-Interim: New ECMWF reanalysis products from 1989 onwards. *ECMWF Newsletter*, 2007, 110: 25-35.
- 22 Dee D P, Uppala S. Variational bias correction of satellite radiance data in the ERA-Interim reanalysis. *Quarterly Journal of Royal Meteorology Society*, 2009, 135:1830-1841.
- 23 Randall D, Curry J, Battisti D, et al. Status of and outlook for large scale modeling of atmosphere-ice-ocean interactions in the Arctic. *Bulletin of the American Meteorological Society*, 1998, 79: 197-219.
- 24 Ek M B, Mitchell K E, Lin Y, et al. Implementation of Noah land surface model advances in the National Centers for Environmental Prediction operational Mesoscale Eta Model. *Journal of Geophysical Research*, 2003, 108: 8851, doi:10.1029/2002JD003296.
- 25 Pleim J E, Xiu A. Development of a land surface model. Part II: Data assimilation. *Journal of Applied Meteorology*, 2003, 42: 1811-1822.
- 26 Xiu A, Pleim J E. Development of a land surface model. Part I: Application in a mesoscale meteorological model. *Journal of Applied Meteorology*, 2001, 40: 192-209.
- 27 Hogue T S, Bastidas L, Gupta H, et al. Evaluation and transferability of the Noah land surface model in semiarid environments. *Journal of Hydrometeorology*, 2005, 6: 68-84.